CHAPTER 5

CAMERA CALIBRATION CASE STUDIES

Executive summary

This chapter discusses a number of calibration procedures for determination of the focal length, principal point, radial and tangential lens distortion parameters as well as some additional lesser-used parameters. The methods discussed range from laboratory procedures to techniques that are used at the same time as measuring an object in 3-D. Finally the selection of the appropriate method for a given application is discussed.

5.1 Determination of the location of the principal point

The method described in Chapter 4 for determining the principal point location was used in a calibration of a number of Pulnix TM6CN cameras. A low power laser was aligned with the centre of the CCD array by causing the primary reflection from the surface of the sensor to coincide with the incident beam (Figure 5.1). Coincidence was identified by symmetry with the diffraction pattern caused by the surface structure of the sensor. Care had to be taken in distinguishing this from the similar strength reflection from the cover glass front surface. Each lens was fitted to the camera and an image grabbed with the laser suitably attenuated. The location of the laser imaged spot by definition coincides with the principal point of symmetry.

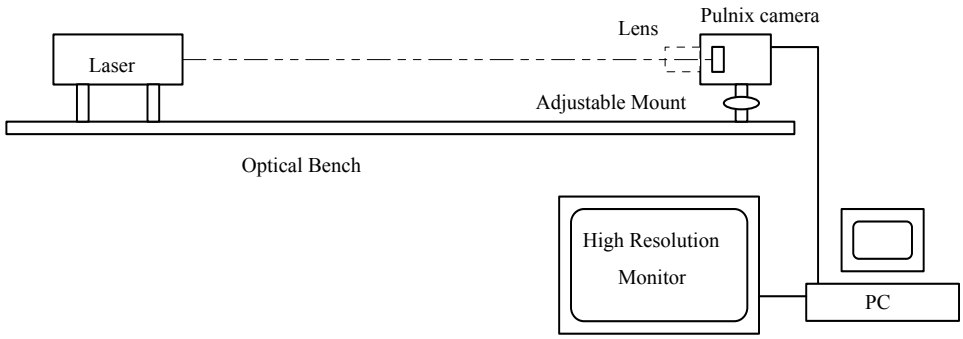

Figure 5.1. Schematic diagram of the principal point location system

A principal point determination repeatability test was conducted. Three operators repeatedly aligned the system using camera 2 and lens 2 focused at infinity. In each case the target image centre was located by visual examination of the image co-ordinate grey values. Results from this evaluation (Table 5.1) show good repeatability between operators. The same method was then used to assess the principal point of

symmetry for each camera and lens combination, mean values are shown in (Table 5.2).

Operator	1		2		3	
Observation	x	y	x	y	x	y
1	350	219	350	219	349	219
2	351	218	349	219	348	218.5
3	351	219	349	219	349	218.5
4	351	218.5	351	219	348	218.5
5	351	218.5	349.5	219	348	218.5

Table 5.1. Lens principal point location repeatability.

Camera	Lens	Principal Point	
No.	No.	x	y
1	1	360.5	268
1	2	354	263.5
1	3	343	275.5
2	2	351	221
3	3	346.5	293

Table 5.2. Principal point measurement with differing lenses and cameras

It is well known that in a real lens the principal point will vary with the lens extension necessary to achieve sharp focus. Such variations were evaluated for one of the cameras by adjusting the lens to five different settings throughout its imaging range. Results are shown in table 5.3, significant variations of 3 pixels in x and 14 pixels in y were noted.

Focus Setting	x	y
Infinity	350	220
5m	349	218.5
2m	348.5	216.5
1m	349	213.5
0.5m	347	206
Infinity	350	220.5

Table 5.3 Variation of lens focus

The location of the principal point can be determined in this manner but unless this parameter is required on its own or other calibration methods cannot be used this method is not likely to be used very often in practice.

5.2 Plumb line calibration of 25 mm focal length C mount lenses

5.2.1. Introduction.

The calibration of three 25 mm focal length lenses using the plumb line method is discussed. In particular variations of parameters with focus and changes in camera required analysis. It should be noted that in this case study the calibrations performed were for a research purposes and many more observations and care was taken than would be necessary for a working calibration of a lens. As a result of the extra experiments it was found that for these lenses a reasonable calibration of the lens could be obtained using four plumb lines just inside the periphery of the image. This was largely on account of the relatively low level of distortion found using these lenses with the sensor format of the cameras.

5.2.2 Setting up

A 1.5 metre square frame of timber with white nylon string stretched tightly across it was used. To provide as much contrast as possible, a backdrop made of black velvet curtains was used. This backdrop was placed 1.5 metres behind the calibration frame so that side-lighting could be used to illuminate the white string and not the curtain (see Figure 5.2 & 5.3). Some difficulty was experienced in obtaining optimum lighting settings in all circumstances because of the conflicting demands of keeping the image in focus and providing enough lighting on the lines, while not illuminating the background. For many of the images it was possible to use natural lighting from a large window that was directly behind the camera.

Figure 5.2. Setting up the camera for measurement

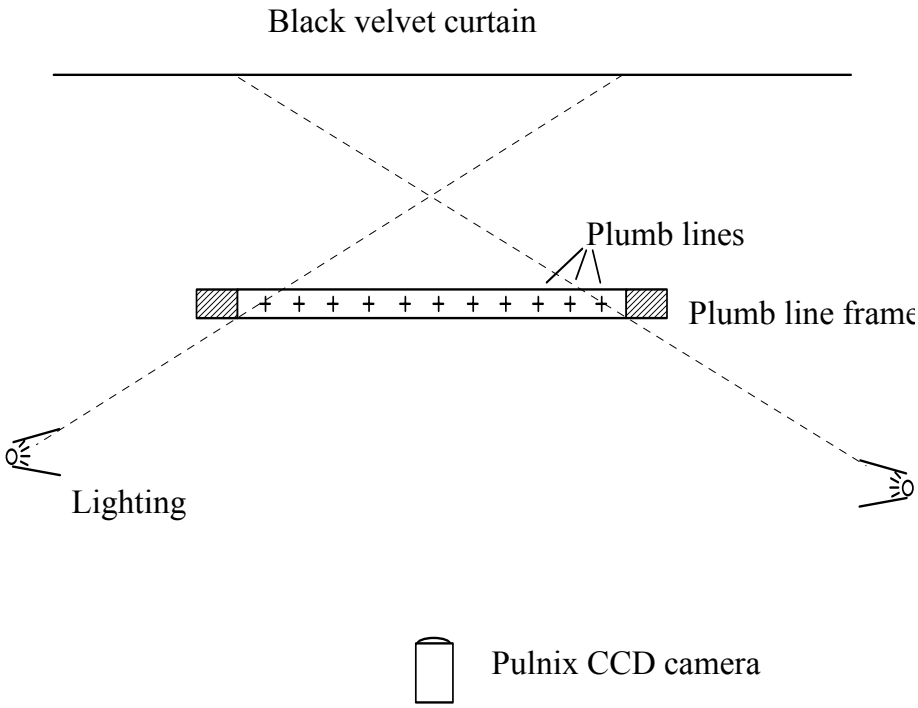

Figure 5.3. The configuration of the lines (plan view)

It was intended that focal length settings of 0.5, 1, 2, and 4 metres would be used. Images were collected at a camera to plumb line distance of 0.5 metres, however, at this position, a problem was noted which originated in the type of string used. Figure 5.4 and 5.5 illustrate that under these conditions the sensor was able to resolve the fine weave of the string.

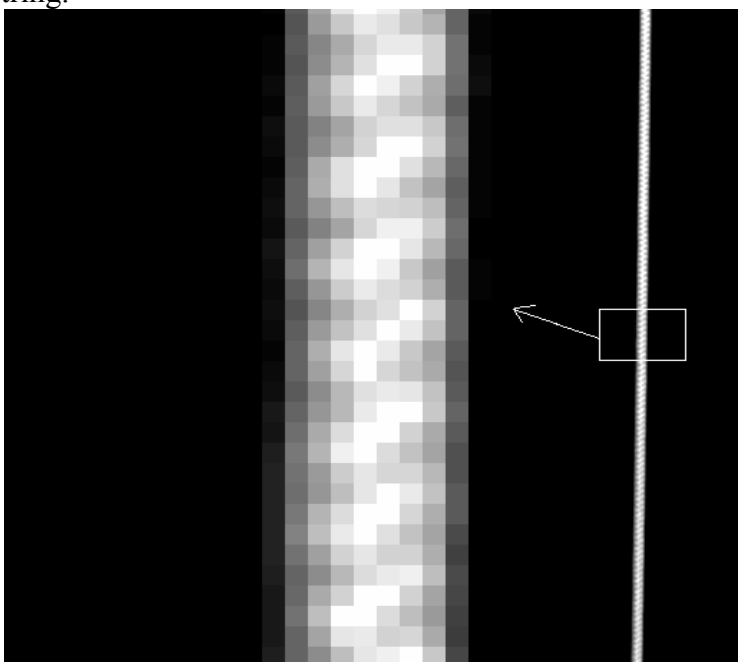

Figure 5.4. Close up view of the string at 0.5 metres

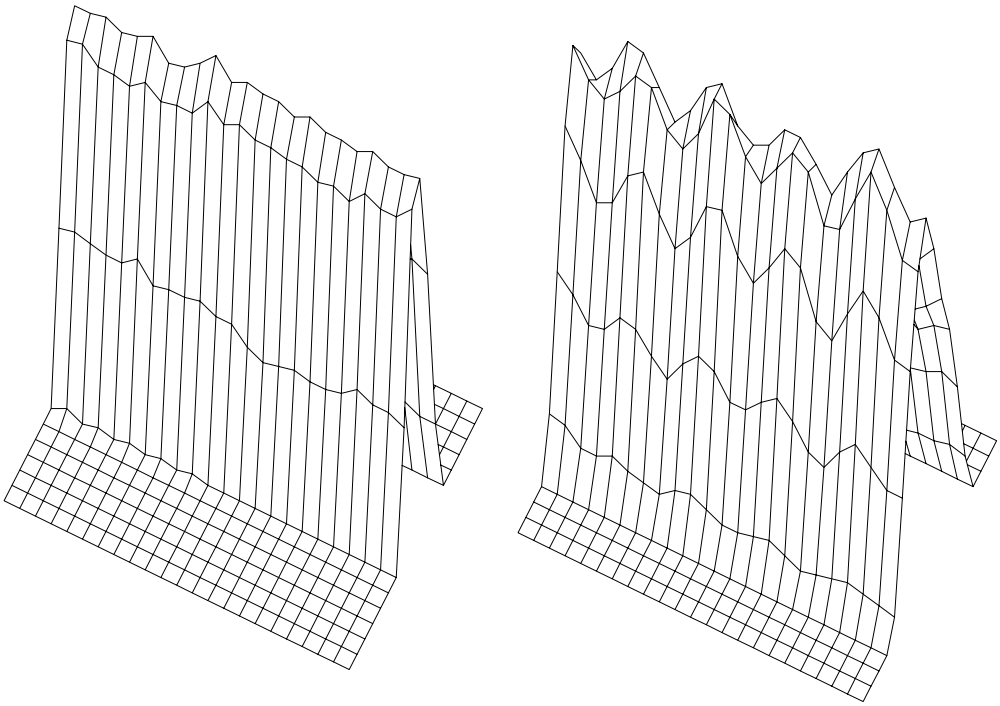

Figure 5.5. A 3-D plot of section of string at 1.0 and 0.5 metres

The result was an unacceptably high level of noise to allow meaningful comparisons between data sets so the experiment concentrated on the results from camera to plumb line distances of 1, 2 and 4 metres.

5.2.3 Results

Three Pulnix TM6CN CCD cameras were each fitted with a, apparently identical, Fujinon 25mm C-mount lens camera to object distances of 1, 2 and 4 metres. Each combination of camera, lens and distance was tested, resulting in 27 determinations of the parameters of radial and decentering distortion. To summarise the results the distortion at 4 mm from the lens principal point was caclulated using the parameters of lens distortion obtained from a least squares estimation program (Tables 5.4 and 5.5).

Camera	**Lens**	**Camera to Object Distance**		
No.	**No.**	**4m**	**2m**	**1m**
1	1	11.9µm	13.8µm	13.6µm
	2	13.7µm	14.3µm	16.0µm
	3	12.8µm	12.6µm	14.8µm
2	1	12.5µm	14.2µm	15.6µm
	2	12.9µm	13.9µm	15.2µm
	3	12.9µm	13.7µm	15.1µm
3	1	13.1µm	14.5µm	16.0µm
	2	13.7µm	14.1µm	17.1µm
	3	12.7µm	13.4µm	15.2µm

Table 5.4. Radial lens distortions in micrometers at a radial distance of 4 millimetres for three Pulnix cameras, three Fujinon 25mm lenses and three camera to object distances, derived using approximately ten horizontal and ten vertical plumblines

Lens No.	Camera t o 4m	Object 2m	Distance 1m
1	12.5µm	14.2µm	15.1µm
2	13.4µm	14.1µm	16.1µm
3	12.8µm	13.2µm	15.0µm
Mean	12.9µm	13.8µm	15.4µm

Table 5.5. Summary of table 5.4, showing mean values for radial distortion in micrometers for a radial distance of 4 millimetres for three Fujinon 25mm lenses fitted to three Pulnix cameras

A graph illustrating the distortion curves is given in Figure 5.6.

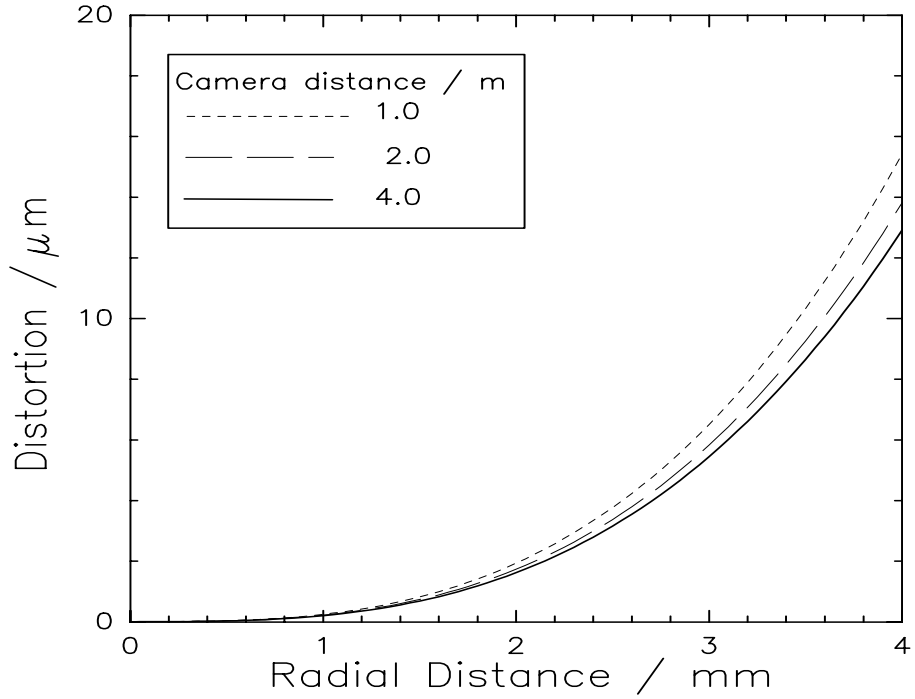

Figure 5.6. Graph of mean results

Several tests were made on this data, probably the most significant being to determine if all the commonly used three parameters for radial distortion were significant for such a, relatively, long focal length lens. The tests showed conclusively that only the first term (the K_1 term, see for example Karara, 1989), was required to describe the 'barrel' distortion effect. This proved to be a most important finding because it enabled a simplified approach to the determination of lens distortion. This technique presents opportunities for the determination of the actual distortions present at the time of image capture.

Inspection of Table 5.4 shows the small range of the results for each focus distance, remembering that three different cameras and lenses were involved. Table 5.5 shows a summary of the results of Table 5.4. Note that the maximum radial distance that it was practical to reach in the corner of the Pulnix CCD frame is only 3.8mm, so extrapolation of the results to 4mm should heighten any real differences in the lenses. Note also that at a radial distance of 2mm, within which most imagery will probably be captured, the size of the radial distortion will be only one-eighth as large as those figures shown in the tables (because the coefficient of K_1 is r^3), so the differences between lenses will be accordingly smaller.

The decentering distortion profiles are shown in summary form in Table 5.6. The increase in decentering distortion for closer focussing is quite understandable, as the lens elements are moved towards the object by approximately 0.30 mm in focusing from 2 m to 1 m, whereas the lens is only moved forward by 0.15 mm in proceeding from 4 m to 2 m focus. Again the values at a radial distance of 4 mm have been shown. Applying the same reasoning as above, if most imagery is captured within a radial distance of 2 mm, this corresponds to a worst case decentering distortion of 1 μm (the decentering distortion coefficient is basically a quadratic term, so halving the radial distance reduces the effect to a quarter).

Plumbline Type	**Camera to Object Distance**		
	4m	**2m**	**1m**
10 Horizontal 10 Vertical	1.5μm	1.6μm	3.7μm
2 Horizontal 2 Vertical	2.6μm	2.0μm	3.0μm

Table 5.6. Summary of values of the decentering distortion profiles in micrometers at a radial distance of 4 millimetres for various camera to object distances for three Fujinon 25mm lenses fitted to three Pulnix cameras

The decentering distortions found were up to an order of magnitude smaller than radial distortion. This agrees with the typical rule of thumb that decentring distortion effects are 1/7 of the value of radial distortion. In many cases these distortions can be ignored and a simple estimate of the maximum distortions acceptable for a given application will enable a decision to be made.

5.2.4 Calibration with peripheral lines

The results of the precise determinations of the lens distortions using the plumbline method with approximately ten horizontal and ten vertical lines showed conclusively that for the 25mm Fujinon C-mount lenses tested, only the first term of radial distortion was significant. It was therefore decided to repeat the entire set of tests using only two horizontal and two vertical lines. These lines were of white nylon string, placed on a wooden frame, not unlike a picture frame, which had been painted matt black.

The data capture was again automatically undertaken, and the results for all 27 tests, that is for three cameras, three lenses and camera to object distances of 1, 2 and 4 metres are shown in Table 5.7. A summary of the results is presented in Table 5.8, where it can be seen from comparison with Table 5.5 that the results are, to a high level of statistical confidence, identical.

Camera	Lens	Camera to Object Distance		
No.	**No.**	**4m**	**2m**	**1m**
1	1	11.1μm	13.1μm	13.9μm
	2	13.2μm	14.4μm	15.6μm
	3	13.9μm	12.6μm	15.3μm
2	1	12.7μm	14.4μm	15.6μm
	2	12.8μm	13.6μm	15.8μm
	3	13.1μm	13.5μm	15.5μm
3	1	13.6μm	14.0μm	15.9μm
	2	14.1μm	14.0μm	15.9μm
	3	13.1μm	14.2μm	15.3μm

Table 5.7. Radial lens distortions in micrometres at a radial distance of 4 millimetres for three Pulnix cameras, three Fujinon 25mm lenses and three camera to object distances, derived using only two horizontal and two vertical plumblines

Lens No.	Camera to Object Distance		
	4m	**2m**	**1m**
1	12.5μm	13.8μm	15.1μm
2	13.4μm	14.0μm	15.8μm
3	13.4μm	13.4μm	15.3μm
Mean	13.1μm	13.7μm	15.4μm

Table 5.8. Summary of Table 5.7, showing mean values for radial distortion in micrometers for a radial distance of 4 millimetres for three Fujinon 25mm lenses fitted to three Pulnix cameras

The utility of this result is that radial and decentering distortions can be determines simultaneously at the time of digital data capture. A frame need only be placed around the object being recorded, and regardless of the amount of focussing (or indeed de-focussing) which takes place, the lens distortions and, in effect, the offsets of the principal point, are determined for that epoch of exposure. This technique will not, of course, suit every application, but in many instances where the camera is placed remotely in a hostile environment and focussing and aperture settings are under automatic control, then this technique could be useful.

5.2.5 Assessment

To test the use of the quick calibration method a number of images of a target test field and the calibration frame were taken. Figure 5.7 shows the target test field and frame, and Figure 5.8 shows one of the images collected for processing. The plumblines were extracted from one of the images and used in the plumbline program to compute an estimate of the K_1 parameter of 2.183 x 10^{-4}. The target co-ordinates for each of the images was then used to compute a bundle adjustment where K_2, and K_3 were suppressed and K_1 was free. The value of K_1 that was produced was 2.098 x 10^{-4}. The small difference of 0.09x10^{-4} is equivalent to only 0.2μm at a radial distance of 3 mm, that is near the practical limit of the image format where the radial distortion effect is at its maximum.

The target co-ordinates were then adjusted using the value of K_1 from the quick method and the bundle adjustment re-computed. The resulting K_1 was 2.258 x 10^{-5}, a factor of 10 less, showing that the major systematic effect of radial lens distortion had been removed. The RMS values for the test field in object coordinates were: x = 0.021mm, y = 0.025mm, z = 0.027mm for both methods. The corresponding values in image space for x and y were both 0.48μm. An overall expression of the accuracy obtained was of the order of 1:16,000.

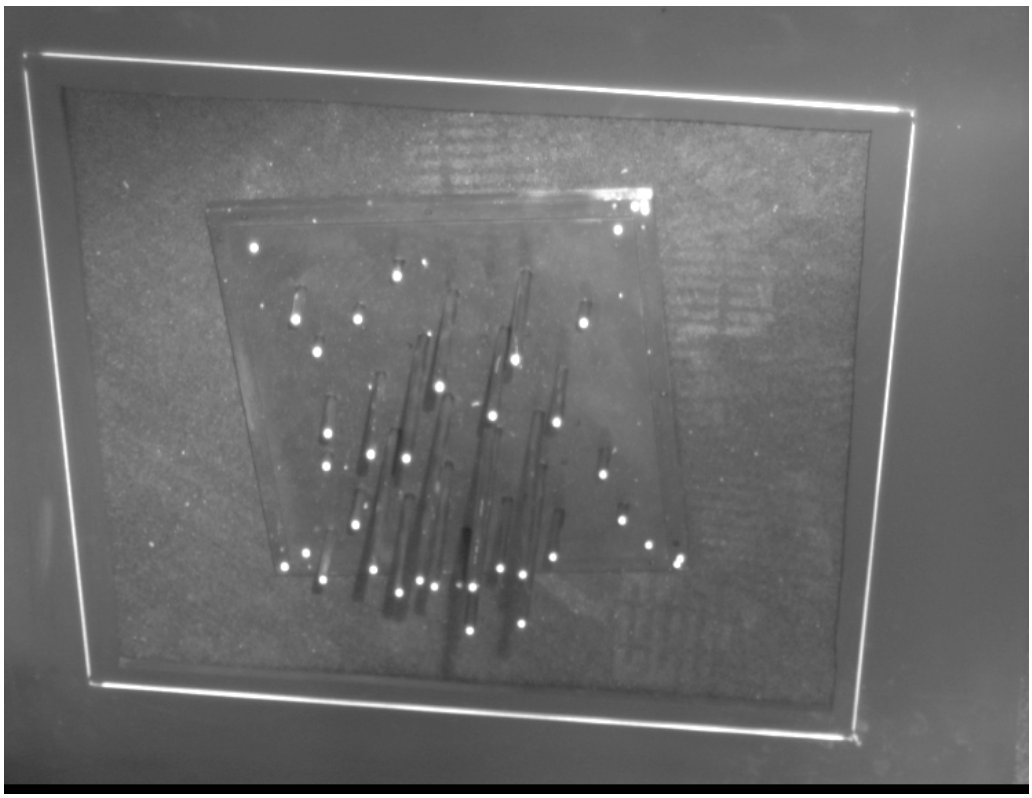

Figure 5.7. Grey scale view of target test field and frame

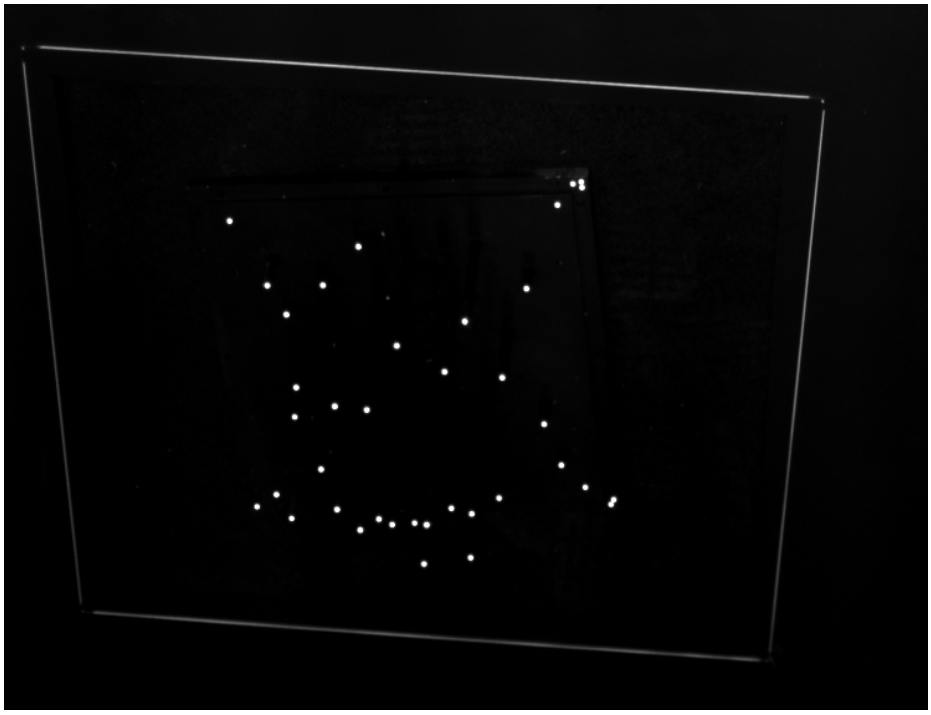

Figure 5.8. Image used to compute K1 and bundle

5.2.6 Conclusion

The radial and decentering lens distortions for three Fujinon 25mm lens fitted to three Pulnix digital cameras were determined by the plumbline method with residuals of the order of 0.2μm. A study of the parameters of radial distortion showed that only the first term in the series was sufficient to describe the radial distortion present in these lenses. Further tests showed that the plumbline test field in the laboratory could be reduced to only two horizontal and two vertical lines attached to a lightweight frame without significant loss of accuracy. Bundle adjustments of a test field incorporating this technique showed accuracy results of the order of 1:16,000. Caution should be used in extrapolating these results to shorter focal length lenses where the radial distortion has been shown to be up to an order of magnitude larger than the lenses tested here (Beyer, 1992).

5.3 Aerial Camera calibration in situ (230 x 230 mm format film)

5.3.1 Scenario

A national mapping agency had used the services of the national measurement laboratory to calibrate its aerial cameras on a goniometer owned and operated by that national measurement laboratory. This goniometer had obviously been purchased after World War II, at a time when government departments had no need for cost justification and micro-economic reform wasn't even mentioned in text-books. The device worked just fine, and produced results which no-one questioned as post-war mapping was a national priority. In the days of analogue/mechanical stereoplotters (and before computerised solutions for photogrammetric aerial-triangulation), the best accuracy one could expect for most operations was of the order of 10 μm. For contouring it was probably closer to 20 μm if an operator could remove 'y-parallax' to within half the width of the floating mark which was used to follow the terrain.

By 1980, several problems arose. The measurement authority was undergoing a review and realised its old goniometer was only rarely being used (one calibration a year at most), it occupied a whole laboratory and mapping was no longer a national priority. It was offered to the national mapping agency whose director accepted it, but did not realise that aerial cameras had changed significantly in the previous thirty years. No longer were focal lengths a 'standard' 150mm which fitted nicely onto the goniometer, but rather were a wide-angle 114 mm or even a super-wide angle 87.5mm. The modern cameras and lenses could only be tested on the goniometer after considerable re-fabrication to the camera mount and frame.

When calibrated in the new, temperature controlled (20^{o}C), laboratory, the camera/lens distortion curves seemed to be up to 40 μm different from values which were now being obtained from calculations based on photography taken over a 120 point ground-based test range. Ground targets consisted of the centres of round-abouts and other street intersections and were quite well-defined. What was wrong?

5.3.2 In-Situ Plumb-line Calibration

One of the suspicions was that there was a temperature effect that may be causing the radial distortion. This eventually proved to be a factor as the air temperature around the lens was as low as minus 20^{o}C at the time of photography. The reliability of the lens distortions based on the ground test-range were subject to some doubt as only vertical or near-vertical photography of the substantially flat (or 2-D) test range were possible. It was not possible to replicate the efficient multi-image solution of a laboratory test-range for small format cameras where convergent angles up 90^{o} could be made between exposures. In fact, the aerial camera would not operate if tilted by more than a few degrees! Suspicions of 'projective compensation' between the results for the lens distortions and the slight angles of camera tilt were raised as a possible error source by those still defending the goniometer calibration.

Eventually a perfectly straight section of railway line, approximately 10 km in length and possessing only minimal changes in grade for which heights were known, was found and photographed with multiple exposures across all portions of the image format. Photography was performed by both north-south and east-west runs to make

this the world's largest-ever plumbline calibration. After correcting the digitised images of the railway line for slight height relief effects, the lens distortions were computed and confirmed the previous test-range results. Why were the goniometer results still so different?

After considerable "detective work", it was decided to investigate the flatness of the image platen. This is the metal backing plate which holds, via vacuum suction through tiny holes, the film "flat" at the time of exposure. When testing on the goniometer, a grid plate was placed into the image plane and the back of the camera completely removed so that the grid crosses could be illuminated and seen through the viewing "theodolite" arrangement.

The platen proved to be quite concave, so that when it was applying a vacuum, the film was actually introducing its own form of radial distortion to the imagery. When this curved platen effect was added to the distortions revealed by the goniometer tests, the results disclosed more than half of the "missing" radial distortion determined from the 'in-situ' tests. Temperature in air versus temperature in the laboratory was seen as the cause of the missing component. The goniometer was never used again for aerial calibrations.

5.4 An aerial camera calibration for lens distortion and focal length(120 x 100 mm format film)

5.4.1 Scenario

A private surveyor purchased a Linhof 5 inch by 4 inch aerial survey camera. It appeared to be in good working order and came with nominal 90 mm and 150 mm lenses. Was it really in good condition or had it been "knocked around"? Could it be used for surveying purposes such as investigations for new country roads? The surveyor was contemplating using it with either an analytical or digital stereoplotter. This was significant because it meant that a determination of the principal point was not required, only lens distortions and focal length. To determine the principal point, either an elaborate laboratory set-up is required or a multi-station convergent bundle adjustment. The former was not available, and the latter would be very difficult for lenses which were focussed at infinity.The manual that came with the camera seemed to indicate the lenses worked best from a minimum camera-object range of 30 metres. The camera was really quite heavy, and any hand-held operation would be best left to Olympic weight-lifters!

5.4.2 In-Situ Plumb-line Calibration and Focal Length Test

A very heavy-duty television camera tripod was acquired and the Linhof fortunately had one spare screw hole to which attachment was possible. The 24-volt power supply was found to be aged and a 'jury-rig' running from a car's cigarette lighter improvised so that the motorised wind-on and vacuum system could be activated outdoors. A bank building, situated on a street corner, four storeys high with a total facade of large vertical glass plates was found 'down-town'. The diagonally opposite street corner had a building which was slightly set-back from the building alignment, so it was just possible to get about 30 metres camera-object distance.

The vertical glass panels had approximately 25mm gaps between one another and by looking up the facade, appeared to be very well aligned. An outdoors plumbline range had been established! The photography went smoothly, including rolling the camera through 90^{o} so that 'horizontal' as well as 'vertical' lines could be imaged. Controlling the crowd was a slight distraction as the presence of a truly big camera on the footpath, especially with the 150 mm lens fitted, and hard-wired to the car's cigarette lighter, caused several camera enthusiasts to gather.

The radial and decentering distortions could now be easily handled via standard routines for digitising the edges of the glass panels and running through plumbline software. It is noteworthy that the camera does not have to be at right angles to the plumblines. The camera was severely tilted at the time of photography (perhaps 30^{o}), but this is also irrelevant. Plumbline calibrations at infinity focus only require the lines in object space to be straight : nothing more.

Two soccer fields, side by side, proved to be the answer to the focal length determination. The ends of the fields were in a straight line, so the distances between the four goal posts, one set on each field, were measured to the nearest centimetre (total distance approx. 70 to 80 metres). Two distances were measured by taping down the gap between the soccer fields to two points from which the far goal posts

could be seen with the 90 mm and 150 mm lenses. These distances were about 90 and 130 metres from the line of the goal posts. Photographs were taken with a determined effort to keep the camera level and the goal posts to appear on the horizontal axis of the image plane.

The image positions of the goal posts were measured on a mono-comparator across the centre of the image (important so that no angular corrections are required). A correction for the effect of radial distortion was applied to each image location. By very simple ratioing of distances between targets to camera-to-object distances, values for the focal length of the lenses could be calculated. Since four goal posts appeared in each image, different combinations were used to calculate the focal lengths and the means adopted.

Given that the target distances (goal posts) were measured in the field to 0.01m in approx. 100m and the image coordinates were observed to approx. 0.01mm in about 100mm, the the calculated focal lengths could be quoted to the nearest 0.01mm, a most satisfactory value for aerial survey work. The simple geometric principles of photogrammetry should never be forgotten.

The results for the radial distortion were really outstanding. The distortion curves remained below a value of 20 μm until near the edge of the format, a result which indicated that the lenses were of a high quality. Unfortunately, the parameters for decentering distortion for the 90mm lens were much larger than would be expected. The decentering distortion profile approached 60 μm towards the edge of the format. This is at least twice as high as could reasonably be expected and indicates that the lens elements had suffered some rough treatment at some time in the past. For analytical and digital processing of imagery from these lenses, this was not considered to pose a problem for the use of this camera.

5.5. A small format camera for aerial photographic purposes (60 x 60 mm format film)

5.5.1 Scenario

A government department is charged with the task of monitoring coastal sand-dune erosion. The strip of coastline involved is approximately 1000 km in length, but only up to 300 metres wide. A small format 60 x 60 mm (Hasselblad or Rollei camera) is suited to this task as a light aerial survey plane operated by one-man can economically be used. The calibration of the camera for radial and decentering distortion and focal length is required. A most important consideration is that the filter used during the photography of bright yellow sand dunes is in place during the calibration procedure. Each additional glass element (even if it is flat) will affect the calibration result. In this case a reseau plate has also been fitted to the Hasselblad camera, both to provide a medium to contain film bulging (no vacuum in this camera) and to provide an indication of film deformation which may occur during development.

5.5.2 In-Situ Plumb-line Calibration and Focal Length Test

A 'down-town' building, three storeys high, with a facade consisting of vertical glass panels was found in a pedestrian shopping mall. The building opposite was two storeys high and an approach was made to the occupier to allow photography from the second storey window across the mall. In this way, the camera could be held horizontal on a tripod (checked by a carpenter's spirit level), and at right angles to the glass panels. Images were taken in both the normal and rolled positions. The distance across the mall, building to building, was measured by taping, as were the distances between the glass panels.

The photography was analysed in the usual manner for the parameters of radial and decentering lens distortion by digitising lines along the edges of the panels. Because the camera had been held in a fixed position at right angles to the glass-panelled building and the distance away from that building had been measured, the image distances between certain glass panels could be corrected for radial distortion and the focal length promptly computed by simple geometry.

5.6 Video cameras for close range (under 500mm camera-object distance)

5.6.1 Scenario

There was a need for some cranio-facial imagery to be captured quickly and analysed in an automated procedure by surface matching to produce near-real-time contour plots in a medical environment. Simple analog video cameras, set up in a stereo configuration, and attached to a frame grabber were decided upon, with the only possible variable being the focus setting for the image capture. This would depend on a number of factors, including access proximity to the patient during phases of the surgical operation. In close range situations, radial distortion can vary by very large amounts (say from 100 μm at 500 mm camera-object distance to 300 μm at 200 mm).

5.6.1 Calibration Procedure

The exact value for the principal distance was not crucial to this calibration. Any slight uncertainties in the precise principal distance for a stereo-pair of images would be projectively compensated by an alteration in the assumed distance of the camera to the object. The correction of the radial distortion was the primary consideration. The major difficulty was finding suitable objects which could be used as pseudo plumbline ranges.

The technique adopted was to calibrate the lenses at infinity focus (usually 100 times the nominal focal length is far enough away for this condition to be met) and also to calibrate them at a very close range, say 100 mm. By applying the equations for the change in radial distortion with focus distance, values of radial distortion at any focus distance (often called image scale) could be calculated. These equations have been detailed in Chapter 2.

Fine black ruled lines on writing paper were eventually chosen for the close-up plumblines, with the cameras suspended above the lines by a chemical laboratory retort stand. Algorithms were written which allowed the imaged lines to be automatically extracted and digitised, so that data capture for the plumblines was virtually instantaneous. The capture of the lens distortion characteristics at infinity focus was simply achieved by imaging a set of thick (approx. 1mm) fishing lines stretched from a curtain rod down to piece of heavy timber on the floor. An object distance of 2.5 metres was used, which was more than sufficient for the 12.5 mm lenses. During the actual operational procedure, an approximate valued for the camera-object was keyed in prior to image capture and the appropriate lens distortion corrections calculated before the image matching and DTM generation.

5.7 Photogrammetric calibration of 25 mm CCD camera lenses

To calibrate the same 25 mm lenses described in section 5.2 a photogrammetric self calibration was carried out. The self calibration was performed using three cameras with their respective lenses, in the configuration shown in figure 20, to image a wooden board on which were placed 74 circular retro-reflective targets. By virtue of the GAP bundle adjustment program and an automated target matching procedure, both developed at City University, the calibration could be performed automatically.

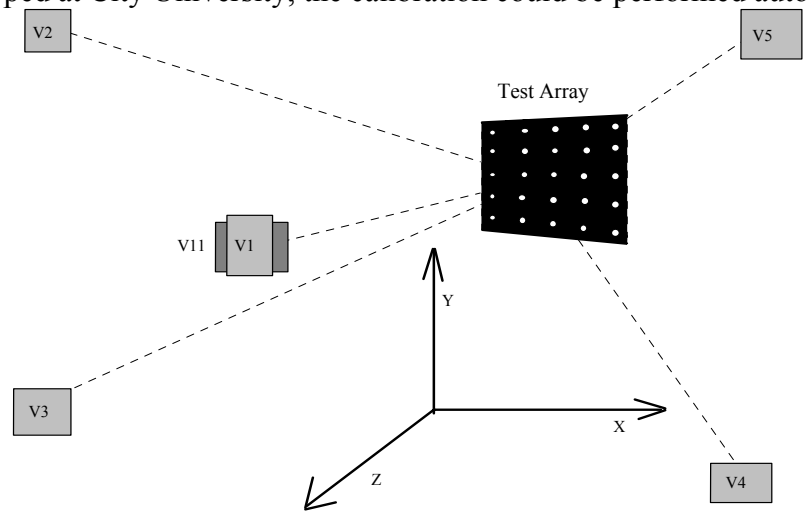

Figure 5.9. The network used for the self calibrating adjustment.

A free adjustment using 6 images per camera such that all 74 targets were imaged at each viewpoint was computed. Camera calibration was carried out for f, x_{pp}, y_{pp}, and lens parameters K_1, P_1 and P_2 for each individual camera. The principal point shifts from the laser alignment were used as *a priori* values constrained by a standard deviation of 3 pixels. All three image sets were combined in a single adjustment with individual camera calibration, such that the 1332 photo-co-ordinate measurements gave rise to 2329 degrees of freedom. Target images were located to subpixel accuracy using a centroid method. These image co-ordinates were then downloaded into the 3D matching procedure to automatically obtain correct target correspondences. The adjustment was then processed using City University's GAP program to give a self-calibrating free adjustment.

Degrees of Freedom 2329	σ_0^2 : 0.303		**No. Measurements** 1332
Co-ordinate axis	X	Y	Z
Target RMS σ	0.0163 mm	0.0210 mm	0.0207 mm
Image RMS residual	0.53μm (1/16 pixel)	0.49μm (1/17 pixel)	---------

Table 5.9. Some parameters from the self-calibrating free bundle adjustment.
0.0205 mm z,x,y rms error

Combination	**Focal Length** (mm)	X_{pp} (mm)	Y_{pp} (mm)	K_1	P_1	P_2
Camera 1, Lens 1	25.107	0.096	0.041	-163.56	-0.050	-0.041
Camera 2, Lens 2	25.022	0.151	0.515	-142.40	-0.070	-0.132
Camera 3, Lens 3	25.011	0.176	-0.066	-132.30	-0.161	-0.017
Standard Deviation	0.010	0.008	0.008	9.57	0.006	0.007

Table 5.10. Some camera calibration parameters and their standard deviations for the Pulnix camera/lens combinations.

The calibration has demonstrated that high precision results can be obtained using small numbers of digital images given an *a priori* knowledge of the performance of individual elements of the digital imaging system.

5.8 Deformation analysis of a series of wood panels over prolonged period

Introduction

The application of this system to deformation analysis of wood panels brings together results of recent research in art conservation and the digital photogrammetric measuring system which has been described in this thesis. A deformation analysis of movement occurring in wood panels was required by the Hamilton Kerr Institute (HKI), University of Cambridge, where a number of wood panels used for supporting fine art paintings were being tested. These panels may swell and shrink as a result of changes in the humidity or temperature of the surrounding air. Effects are amplified in the case of panels painted on one side only because moisture penetrates the two surfaces of the panel at different rates. To obtain the characteristics of the various panels is very important because they are widely used and few systematic studies have been carried out. Different types of wood have different characteristics. A lack of knowledge about the effect of the many different types of reinforcements applied to wood panel paintings to prevent deformation has sometimes led to increased local deformation of the surface and even splitting, cracking, and loss of paint. Therefore it is critical that a method of measurement of the panels is devised to give accurate information about in-plane and out-of-plane deformation. The task for the application here is to use the measuring system to obtain this information for quantitative analysis so that the restoration
options for each panel type can be decided.

The panels to be measured were divided according to wood type: linden; oak; poplar; and Scots pine. Each type was supported by a number of different reinforcement types to give 74 pane; reinforcement combinations.

An Epix frame grabber and Five Pulnix TM6CN camera were used, four of which were located on the four corners and one in the centre to ensure to a minimum of three projections of each target even if the panels be same considerably bent during the experiments. Four 8.5mm lenses and one 6.5mm lens were used to achieve good fields of view from all camera location.

System Calibration using laboratory methods

Laboratory calibration was used to determine each camera principal point of symmetry, radial distortion and decentering distortion parameters. The determination of principal point of symmetry was carried by the method described in section 5.1. The distortion parameters for the four 8.5mm lenses and the single 6.5 mm lens were determined by the plumb-line method. The distance between the camera and plumb line frame was adjusted to the appropriate distance to be used in practice.

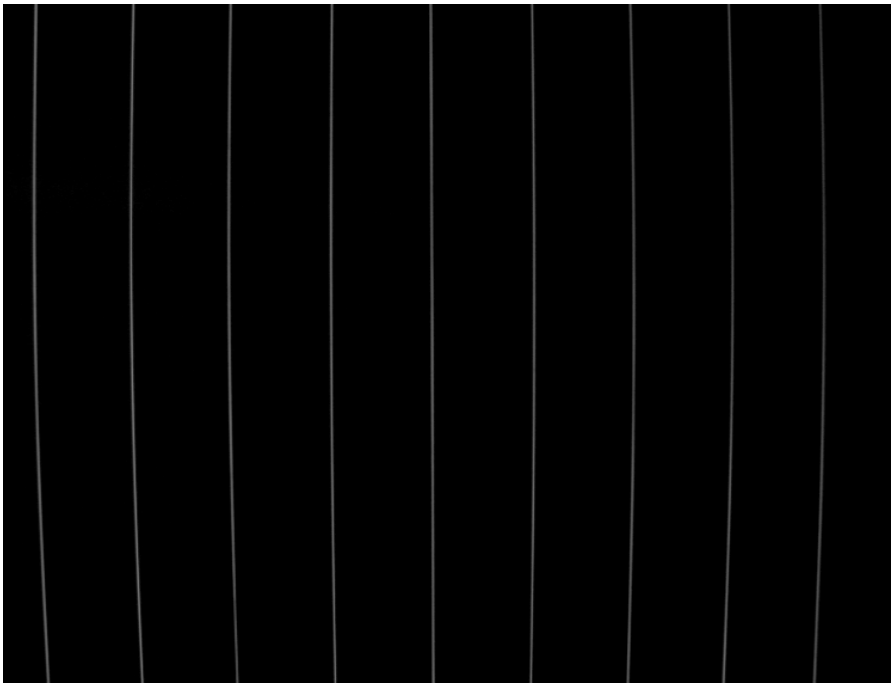

Figure 5.10. Plumb line image

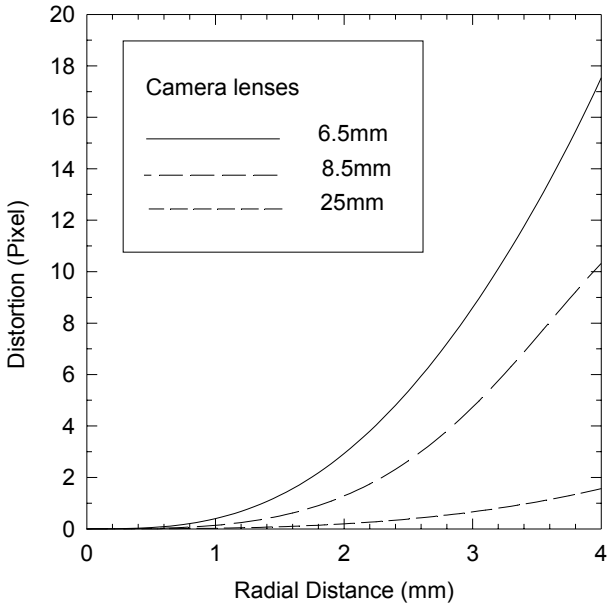

Figure 5.11 Radial lens distortion curves for three lenses

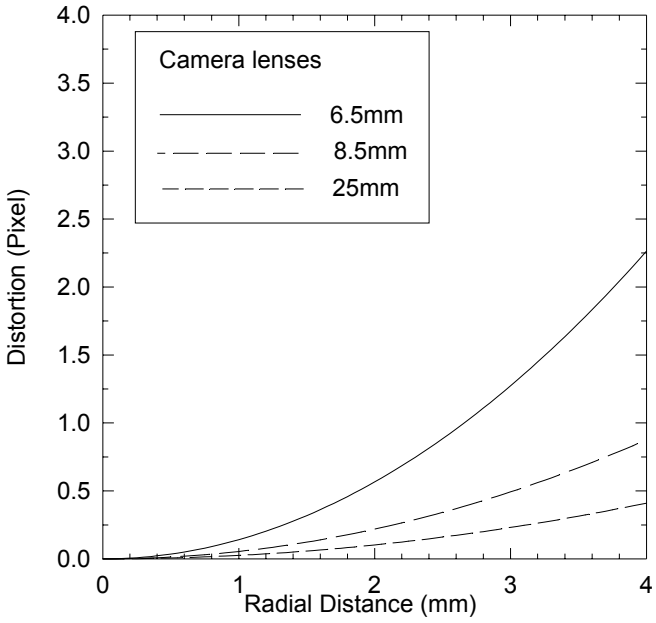

Figure 5.12. Tangential lens distortion curve for three lenses

From the figures, the following information can be obtained: the radial and decentering distortion of the five lenses was far larger than that of 25 mm lenses discussed in chapter three; the four 8.5 mm lenses have very similar radial distortion characteristics and very different decentering characteristics; the 6.5 mm lens has very large distortion, up to 17 pixels shift on the sensor edge to the extent that the distortion can easily be detected by eye. Radial distortion still dominates all distortions when compared to decentering distortion and the numerical value of radial distortion is about ten times larger than that of decentering distortion. However the decentering distortion cannot be ignored because it still represents a maximum of 2 pixel shift for the 6.5 mm lens and 1 pixel shift for two of the four 8 mm lenses.

Self-calibration on the job

A self calibration computed using the test field (Figure 5.13) was used to estimate the camera lens focal length and camera orientation parameters before the panels were measured.

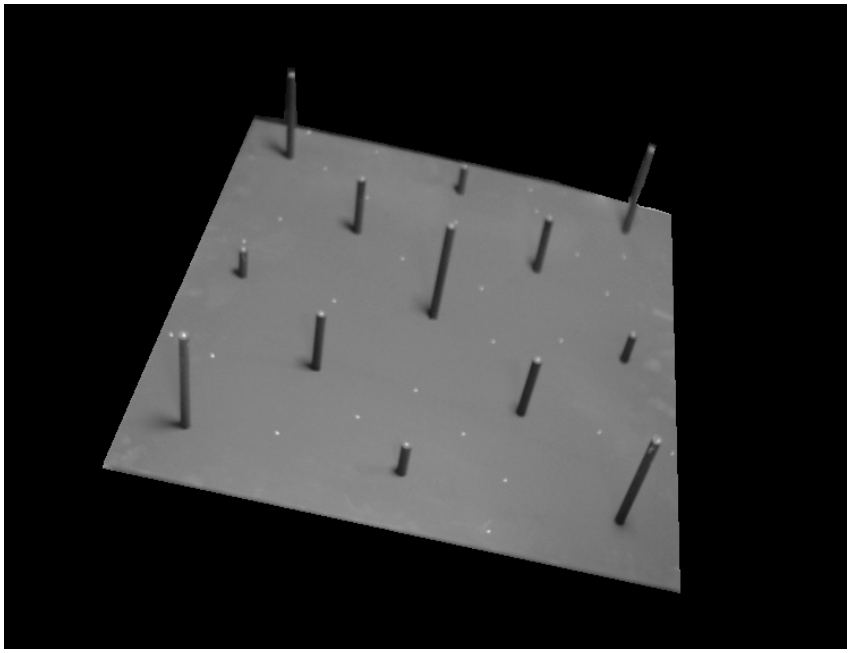

Figure 5.13. 3-D test field using in calibration

The test field was grabbed four times by each camera. Each time the test field was rotated through 90 degrees so that a very strong geometric network was obtained. The targets on each image were automatically located by the location algorithm. Four specially coded targets, were manually identified to estimate the camera orientation parameters. Using this estimation, the 3-D matching algorithm and iterative with bundle adjustment were used to match all the targets on each of the views. The bundle adjustment was run to refine the camera orientation parameters and the 3-D co-ordinates of targets. The focal length parameter was then freed. The focal length of each camera lens may be held fixed from this calibration. However, the camera orientation parameters are likely to change slightly between measurement sets and should remain free. Therefore, at the beginning and the end of each set of measurement the test field was imaged by each of the five cameras and refined camera orientation parameters computed.

A double-walled portion of a workshop at the Hamilton Kerr Institute, with an approximate floor area of 2.8 m x 2.8 m was sealed with walls of thick polyethylene sheet A rack was constructed to hold and adjust the panels to be measured. Four scale bars were installed on the four edges of the panel for scale reference for each measurement. An air temperature of about 20 degrees Celsius controlled by thermostats and electrical heaters. Relative humidity was maintained at regimes of 40% or 80%, +/- 5%, so that a difference of about 40% could be applied for the experiments. A humidifier and dehumidifier, stabilised to the desired level with salt solution, were used to control the humidity, A small fan maintained slow air-circulation.

An array of retro-reflective target were placed on each test panel The number and disposition of the targets on each test panel varied from 157 to 464 according to the pattern of auxiliary supports, see figure 5.14.

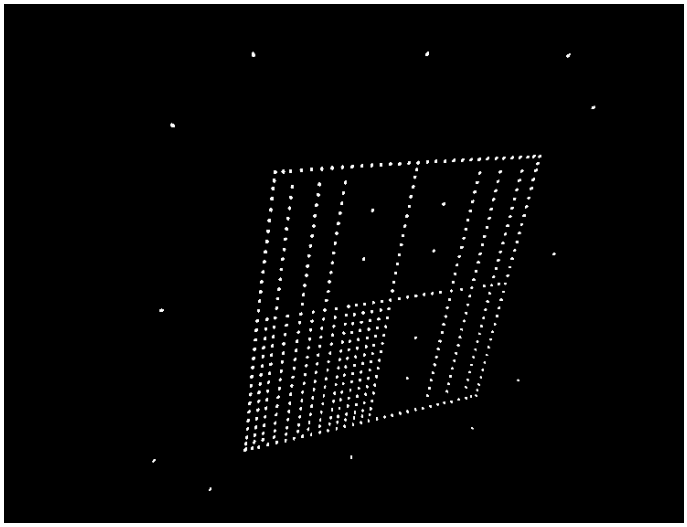

Figure 5.14. Example of the diversity of target locations

An example of a panel during the measurement process are given in figures 5.15 and 5.15.

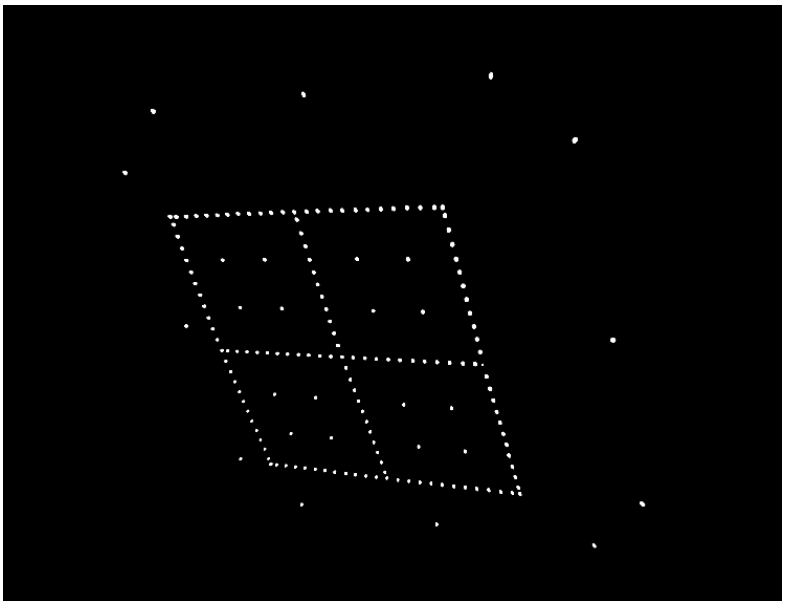

Figure 5.15. Example panel before humidity change

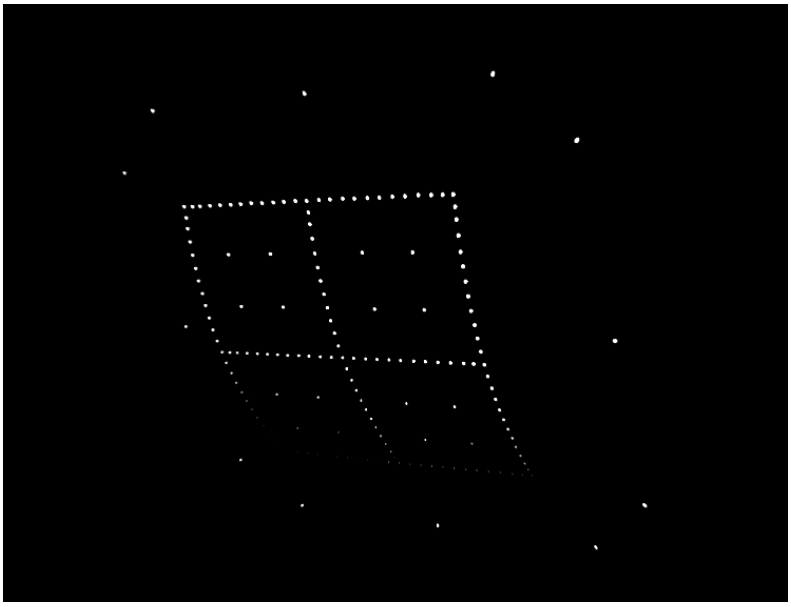

Figure 5.16. Example panel after humidity change

The total number of epochs at which the initial set of images of the 74 test panels would be acquired was 25. For each epoch, there were about 400 images in total to be grabbed, which occupied about 170M storage. During every three epochs, some panels were chosen for quick data acquisition where sequential images were grabbed over very short time, for example one minute between each measurement. Therefore, over 10,000 images grabbed and processed. The average number of targets on each test panels was 250, resulting in a total of 2,500,000 targets to be processed. Obviously for this huge amount of data processing was only feasible if automatic methods were used. In practice each panel was placed in the middle of the support frame. The grabbing of the five images could be automated for all five cameras, but the background of the panel would receive four times the illumination in this way. To avoid background illumination, five images were sequentially grabbed by manually switching on and off the lighting installed on the front of each camera.

During the period that the test panel was swapped for another, the five images grabbed were automatically saved and all the target images on each image were automatically located. The procedure was repeated until images of all panels were grabbed. About 1.5 hours were required for each epoch. All images were then compressed and put into an archive file for future use. The 2-D co-ordinate data of each image were transferred to City University for further data processing. In operation each camera had to be used at least once for each test panel. The five images are grabbed and saved with appropriate file names based on the panel name and the epoch number. The whole process of target image 2-D location was automatically executed without any human intervention.

Data process and analysis

In order to analyse the deformation of the wood panels, there are two steps are necessary after all the 2-D target images co-ordinates have been collected: the target image labelling and 3-D data analysis. Target image labelling includes target image uniqueness matching between different views in each epoch for each panel and the target image uniqueness matching between different epochs for the same panel. 3-D

data analysis includes: the refinement of the 3-D co-ordinates of each target; the comprehensive statistical tests of hypotheses about the quality of the data; and an analytical and graphical display of the deformation of each panel.

The 3-D matching method has been used for uniquely matching target images between different views in each epoch for each panel. The performance of this method has been discussed in chapter five. The problem encountered in this application is the targets on the panel are very close, some targets as close to each other as 20 mm. Ambiguities were possible because the camera orientation estimation was not accurate enough and the computation cost was too high to iteratively match the all target images for the bundle adjustment (for example, the use of 464 targets in a panel will require about half an hour for each iteration of the bundle adjustment). Therefore, an attempt has been made to try to get both camera interior and exterior parameters as accurate as possible. The five camera interior parameters were carefully calibrated by use of the plumb line method, optical bench calibration, and the use of a test field described in previous section. The camera exterior parameters were estimated by using the test field at the beginning of each measurement for each epoch.

The matching algorithm was called twice. In the first call, a group of three for the threshold of target matching was chosen because in some circumstance where the panels were extremely deformed some targets on one side of the panel edge were occluded from the two of the cameras located on the other side. A small 3-D distance tolerance value was chosen to give a strict constraint for target matching. An average of over 90% of the total targets were matching in the first matching procedure. In the second match, the 3-D tolerance value can significantly increased, because the remaining unmatched targets were reasonably sparse in their distribution. Hence, the remaining target images are expected to get matched and labelled. It is emphasised here that the series of experiments are currently ongoing so that is difficult to guess what will be achieved by the end of the project. In order to ensure that targets have identical labelling between different epochs, the data needs to be processed after matching between the different views in the same epoch. Each target on the scale bar can be identified using the space projection method. This is because the scale bars were firmly constructed and the 3-D co-ordinates of each bar target can be precisely obtained. Each camera was also fixed in the same location such that the exterior parameters of each camera could be consistently used for each epoch. The scale bar targets could be uniquely identified by reprojection because their co-ordinates were approximately known and they were imaged in uncluttered regions of each image. The scale bar target images were used as scale constraints in the bundle adjustment procedure so that the size of each panel in each measurement could be determined. The only change between epochs was the position of the same panel in each object space because the panel had to be taken off and put on again some object space shift of the panel position occurred.

The matching of targets between different epochs was based on the principal of similar triangles. The panel could have be expanded or contracted between measurements at each epoch and could also have a significantly different shape. However, any local triangular relationship will still be very similar. Based on the properties of triangular similarity, the matching of targets between each epoch can be achieved. The matching procedure is described as follows. Assume there are two targets, which are physically close in both data sets. Given two targets in the first

dataset, a third target, which is the nearest in space to the two targets, can be found. A triangle linking the three targets is constructed. In the same way, two targets in the second dataset can also used to construct a triangle by combining them with any one of the other targets. From all possible triangles, the one which most closely coincides with the triangle constructed by the first dataset is chosen as correct one. The corresponding third target in the second dataset can then be matched to that in the first dataset.

At some time, some targets were missed in some of the epochs. To minimise the number of unmatched targets, a threshold was used by which only the target lying inside the threshold distance are considered as the matching candidates. The search is extended by selecting the next two closest targets in the first dataset as the basis for the next triangle.

5.9 The use of pre-calibrated lenses

An investigation into the effect of weighting in redundant least squares estimation provides a useful case study into the camera calibration process. To investigate weighing a metrology surface plate was used and targets to two distinct levels of brightness resulting in two distinct levels of 2-D accuracy. The effect of weighting the observations in the least squares process was then observed by fitting a plane to the 3-D data and calculating the standard deviation of the Z component of the data.

Four separate Pulnix cameras were used that had previously been calibrated using a test field rotated about the camera's optical axis and its position altered in such a way as to mimic rolling the camera about its axis by 90 degrees. A self calibrating bundle adjustment was then computed to estimate the camera exterior and interior parameters. This process would typically result in r.m.s. image residuals of the order of 1/20 to 1/40 of a pixel. The cameras were mounted on mounts that would be reasonably rigid but which would be likely to move slightly when cables were taken in an out. The lenses had been set to an appropriate aperture and focus for retro-reflective targets and were taped up using electrical tape.

The measurement of the surface plate took place an unknown number of months after the cameras were calibrated. To perform the measurements four images were collected, one from each camera. To illustrate the process a representative section of the image data are given in table 5.8.

Image Number	Target Identity	X image location (mm)	Y Image location (mm)	Maximum itensity	Area of target
1000	0	-0.408063	0.671105	255	41
1000	1	-0.726981	0.66188	255	43
1000	2	-0.109	0.655554	255	41
1000	3	0.207089	0.645173	240	40
1000	4	0.502227	0.641262	255	37
1000	5	0.801591	0.632442	242	35
1000	6	1.076629	0.627332	213	32
1000	7	1.356481	0.616491	166	31
1000	8	1.636877	0.615434	161	31
1000	9	-0.313232	0.512414	32	13
1000	10	0.014275	0.504681	30	13
1000	11	-0.614753	0.49756	23	13
1000	12	0.312349	0.491477	27	10
1000	13	0.594753	0.48171	14	6
1000	14	1.157856	0.482816	9	6
1000	15	1.4483	0.470817	5	4
1000	16	0.889452	0.460787	14	8
1000	17	-0.808907	0.352273	255	42
1000	18	-0.492438	0.352906	255	41
1000	19	0.707266	0.348713	192	31
1000	20	-0.181772	0.346977	255	39
1001	0	0.255649	2.152449	136	29
1001	1	0.700085	2.149736	165	28
1001	2	0.034017	1.988247	177	30
1001	3	0.475634	1.986422	178	30
1001	4	0.945274	1.97227	183	32
1001	5	-0.197052	1.828331	163	28
1001	6	0.945	1.8122	2	2
1001	7	0.255611	1.823146	174	31
1001	8	0.71194	1.814004	183	31
1001	9	1.155799	1.814822	188	34
1001	10	-0.417689	1.668495	205	34
1001	11	-0.1848	1.6482	3	1
1001	12	0.266	1.6482	4	2
1001	13	0.71736	1.64	3	2
1001	14	0.935605	1.659235	213	31
1001	15	1.1712	1.64	4	2
1001	16	0.028687	1.64995	184	31
1001	17	0.490723	1.646008	198	31
1001	18	1.418874	1.630425	225	35
1001	19	-0.661275	1.496809	219	34
1001	20	-0.433569	1.482938	6	3
1002	0	-0.505829	2.070263	100	27
1002	1	-0.229594	1.969988	117	28
1002	2	-0.97454	1.952488	121	27
1002	3	-0.700366	1.853674	105	27
1002	4	0.030027	1.852953	158	28
1002	5	-0.21	1.8122	2	1
1002	6	-0.9324	1.7876	2	1
1002	7	-1.156577	1.738794	141	27
1002	8	-0.429166	1.742271	131	31
1002	9	0.317008	1.729196	117	28
1002	10	0.08715	1.681	5	2
1002	11	-0.889742	1.62385	167	30
1002	12	-0.15394	1.621896	136	31
1002	13	0.596965	1.613794	145	31
1002	14	0.3609	1.555657	9	5
1002	15	-1.350133	1.51795	111	27
1002	16	-0.618435	1.495075	162	30
1002	17	0.109471	1.499397	185	34
1002	18	-0.84	1.4678	3	1
1002	19	0.890452	1.487781	157	35
1002	20	-0.1218	1.446714	4	4

1003	0	0.753193	0.682694	255	44
1003	1	0.437203	0.576143	255	42
1003	2	0.662388	0.481987	17	8
1003	3	1.224948	0.4991	255	44
1003	4	0.124184	0.481727	255	40
1003	5	0.329144	0.388234	22	10
1003	6	0.897888	0.398383	255	41
1003	7	-0.16734	0.388171	255	39
1003	8	-0.475723	0.292832	255	39
1003	9	0.584841	0.298784	255	39
1003	10	0.061771	0.2729	27	10
1003	11	1.111123	0.273915	23	10
1003	12	-0.258466	0.190783	27	9
1003	13	0.819978	0.189948	22	10
1003	14	-0.764243	0.198428	255	39
1003	15	0.272856	0.194964	255	37
1003	16	1.378697	0.193161	255	39
1003	17	-0.54593	0.106805	22	9
1003	18	-0.038403	0.116669	255	40
1003	19	0.512739	0.102566	21	8
1003	20	-1.066865	0.106034	245	37

Table 5.8. Sample image data

There were approximately 140 targets visible from each viewpoint so the next step was to compute the correspondences between the viewpoints. To achieve this a variant on the epipolar line method was used. The resulting sorted image data in order of increasing target ID but with the image co-ordinates rearranged are illustrated in table 5.9.

Camera Number	Target ID	X Image location (mm)	Y Image location (mm)	Peak intensity	Area of target
1000	0	-0.4846	0.7053	255	41
1000	1	-0.806	0.6963	255	43
1000	2	-0.1833	0.6897	255	41
1000	3	0.135	0.6793	240	40
1000	4	0.4323	0.6754	255	37
1000	5	0.7339	0.6667	242	35
1000	6	1.0112	0.6618	213	32
1000	7	1.2937	0.6512	166	31
1000	8	1.577	0.6504	161	31
1000	9	-0.389	0.5465	32	13
1000	10	-0.0591	0.5387	30	13
1000	11	-0.6927	0.5317	23	13
1000	12	0.241	0.5255	27	10
1000	13	0.5255	0.5158	14	6
1000	14	1.0931	0.5172	9	6
1000	15	1.3863	0.5054	5	4
1000	16	0.8224	0.495	14	8
1000	17	-0.8884	0.3864	255	42
1000	18	-0.5694	0.3869	255	41
1000	19	0.6388	0.3828	192	31
1001	0	-1.3961	1.0987	254	35
1001	1	-1.6393	0.9077	255	39
1001	2	-1.1467	1.2669	195	33
1001	3	-0.887	1.4476	235	35
1001	4	-0.6496	1.6192	219	34
1001	5	-0.404	1.7914	205	34
1001	6	-0.1815	1.952	163	28
1001	7	0.0516	2.1129	177	30
1001	8	0.2754	2.2785	136	29
1001	9	-1.1744	1.0811	8	7
1001	10	-0.9064	1.2699	10	5
1001	11	-1.3994	0.8959	8	6
1001	12	-0.6554	1.4409	7	3
1001	13	1.0543	0.461	5	4
1001	14	0	0	0	0
1001	15	0	0	0	0
1001	16	0	0	0	0
1001	17	-1.4215	0.71	255	39
1001	18	-1.1686	0.8986	255	38
1001	19	-0.1996	1.6129	246	36
1001	20	-0.913	1.0813	255	39
1002	0	-0.1822	2.0078	117	28
1002	1	-0.4609	2.109	100	27
1002	2	0.0796	1.89	158	28
1002	3	0.3689	1.7657	117	28
1002	4	0.651	1.6501	145	31
1002	5	0.9469	1.5239	157	35
1002	6	1.2304	1.4066	169	34
1002	7	1.5281	1.2775	157	32
1002	8	1.8394	1.1535	167	35
1002	9	0	0	0	0
1002	10	0.1371	1.7172	5	2
1002	11	0	0	0	0
1002	12	0.413	1.5914	9	5
1002	13	0	0	0	0
1002	14	1.2719	1.2366	4	4
1002	15	1.5858	1.0935	3	2
1002	16	0.9791	1.328	7	5
1002	17	-0.657	1.8911	105	27
1002	18	-0.3834	1.7788	131	31
1002	19	0.7532	1.3033	158	32
1002	20	-0.1059	1.6578	136	31
1003	0	-1.5814	0.057	255	36
1003	1	-1.8531	-0.0445	255	35
1003	2	-1.2995	0.1369	245	37
1003	3	-0.994	0.2293	255	39

1003	4	-0.7031	0.3236	255	39
1003	5	-0.3924	0.4189	255	39
1003	6	-0.0987	0.5125	255	40
1003	7	0.2166	0.607	255	42
1003	8	0.5351	0.7138	255	44
1003	9	-1.3785	-0.0397	18	5
1003	10	-1.0711	0.0542	24	8
1003	11	-1.6374	-0.1389	12	5
1003	12	-0.7738	0.1375	22	9
1003	13	0	0	0	0
1003	14	0.1077	0.419	22	10
1003	15	0.4434	0.5129	17	8
1003	16	-0.1616	0.3036	27	10
1003	17	-1.703	-0.3077	238	31
1003	18	-1.4253	-0.2185	255	36
1003	19	-0.2625	0.1473	255	40
1003	20	-1.1359	-0.1328	255	37

Table 5.9 Image data after correspondence

The zero's in some of the columns are there because for that particular image no corresponding target was corresponded in the other images. Many of the target locations appear to be similar to those in the uncorresponded set. This is because the object was flat and where the cameras are in certain alignments the target layout will run from the top to the bottom of each image.

Having corresponded the targets using, in this case, the previously known camera orientations reasonably accurately, the 3-D locations of the targets could be estimated. Given the high redundancy it is possible not only to estimate the 3-D target locations but also adjust the camera external parameters.

The camera external and internal parameters are illustrated in the Table 5.10 and Table 5.11 respectively.

Cam ID	X	Y	Z	ω	φ	κ	f
1	1085.2110	1166.3056	1975.6674	-31.0527	25.1024	-75.3778	16.0
2	-1011.4090	1125.6489	1931.6700	-28.3290	-23.9499	-140.3018	16.0
3	-987.7145	-986.1636	1929.9426	26.8270	-23.6023	-52.5825	16.0
4	1108.2272	-1010.6076	1982.3261	26.9131	25.7431	-118.7510	16.0

Table 5.10 Camera exterior parameters

Cam ID	xp	yp	df	k1	k2	k3	p1	p2	A	B	C
1	7.2933e-2	-3.3933e-2	6.8814e-2	5.0057e-4	1.8058e-5	-1.3329e-6	-7.047e-6	1.2302e-5	6.8671e-3	-1.1260e-4	-2.5461e-5
2	-1.7625e-2	-1.2029e-1	7.8992e-2	2.4590e-4	7.6374e-5	-5.0166e-6	-5.871e-5	-1.2951e-5	7.3467e-3	-1.2027e-4	-9.4725e-7
3	-4.8728e-2	-3.3564e-2	1.3894e-1	4.3736e-4	2.6851e-5	-1.8749e-6	2.697e-5	7.143e-6	6.4226e-3	3.9213e-5	-8.0935e-6
4	2.2225e-1	-3.0664e-2	1.4141e-1	8.2395e-4	-5.6280e-5	3.6708e-6	4.328e-5	1.196e-6	6.9696e-3	2.9314e-5	3.4854e-5

Table 5.11 Camera interior parameters

The results from the photogrammetric adjustment process were as follows. To assess the accuracy with respect to the signal to noise ratio of the targets the lighting was varied between four epochs and the image residuals were noted. Most of the targets were of roughly equal intensity. The surface plate is approximately 460 x 600 mm in dimension.

Average target intensity	Image residuals (microns)	Sub-pixel precision
230	0.187	1/43
150	0.207	1/40
80	0.246	1/33
35	0.456	1/20

Table 5.12 Results from four adjustments with varying lighting

To assess the accuracy as compared to the image residuals that result from the photogrammetric adjustment process the residuals from a plane fitted to the data using LSE was computed for the best case was 1 part in 22,000 of the object maximum dimension. The reported precision from the adjustment equated to 1 part in 33,000. This level of precision is around the best that could be expected from a CCIR format camera especially considering each of the cameras had been calibrated some weeks previously and only one image per camera station was used.

An additional set of targets were added to the surface plate. This time the targets were made from a retro-reflective material that was less efficient compared to the material used for the original targets. In this way target intensities that varied considerably were obtained. The area and peak values for these targets are illustrated in the figures 5.17. and 5.18.

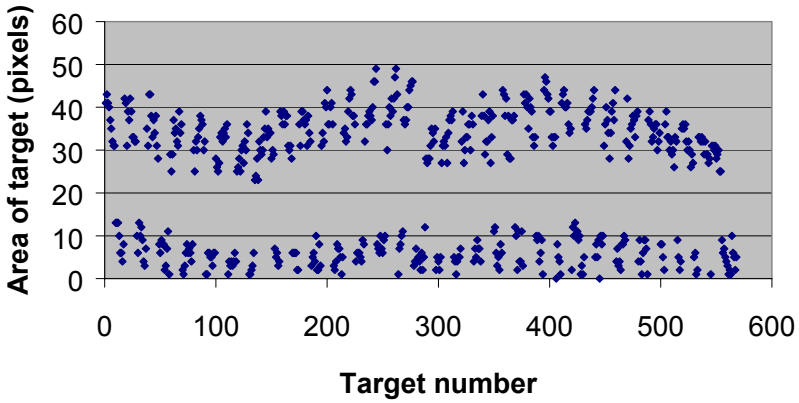

Figure 5.17. Area of targets for the four images

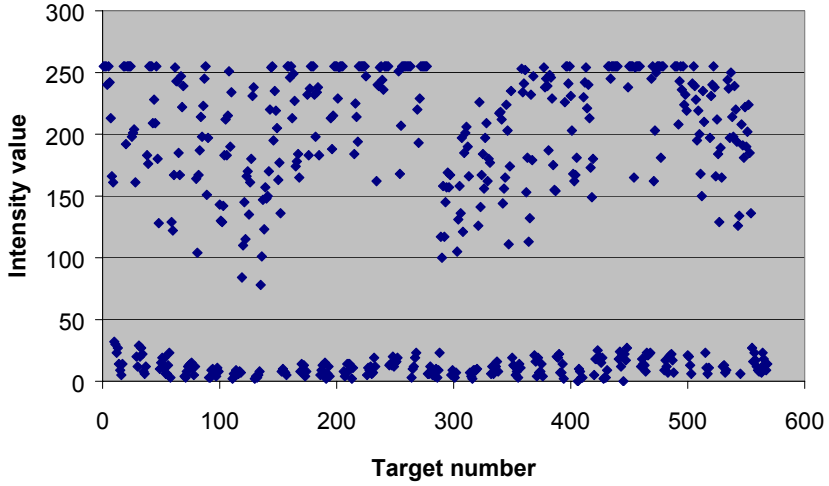

Figure 5.18. Peak intensity of targets for the four images

With such a dramatic variation in size of the images of the targets a clear difference between the two sets was expected to be distinguishable in the final 3-D data. Given that the poor target images were sometimes of just one or two pixels in size, the weighting for the group of targets was chosen to be 3 micrometres and a weighting of 0.3 micrometres was used for the good targets. It may be that these values would not be extreme enough given that an image residual of around 0.2 micrometres is typically achieved for good quality target images. An image of the surface plate is shown in figure 5.19.

Figure 5.19. Image of the surface plate with the high intensity targets (on the white paper squares) and the low intensity targets (circular targets)

A photogrammetric network solution using standard LSE was used to compute the 3-D co-ordinates using the weighting scheme indicated. The results were then sorted according to the reported errors produced by the software. The errors fell into two distinct groups. The in-plane locations of the 3-D data are plotted in figure 5.20 where the triangles represent targets with the smallest errors and the squares represent targets with the largest errors. The in-plane locations of the targets are exactly correlated with the good and poor targets. The 3-D residuals are plotted in figure 5.21.

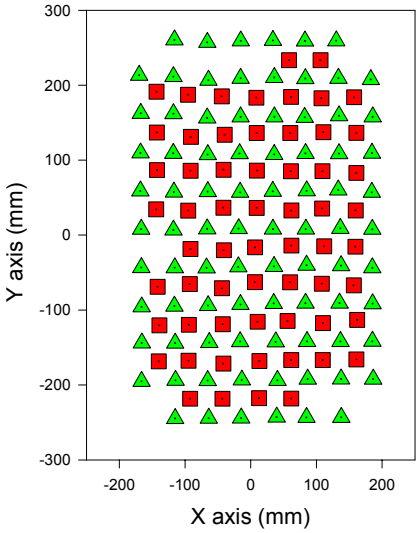

Figure 5.20. Selection of target grouping from error estimates

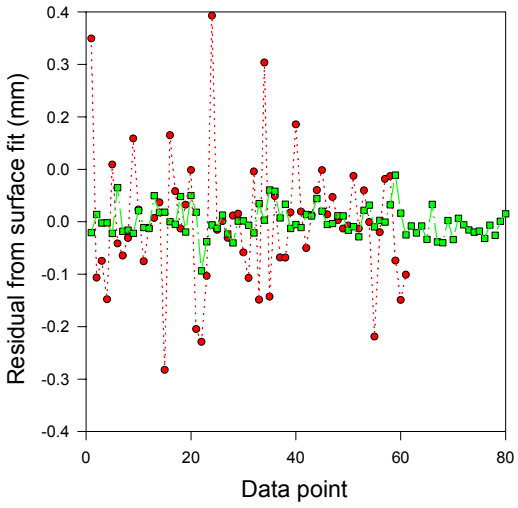

Figure 5.21. Graph of residuals from surface fitting to 3-D data - unequal weighting

A least squares fit of a plane was again performed to analyse these data sets. Given that the surface was expected to be flat it is possible to provide a statistical analysis of the Z coordinate accuracy. The results for the best data were an average standard deviation of 28 micrometres and a RMS error from the plane fitting software of 20 micrometres. For the poor data the results were an average standard deviation of 125 micrometres and a RMS error of 207 micrometres. An accuracy of approximately 1 part in 27,000 is a good result considering that both poor and good measurements were being used at the same time.

This case study illustrates that with the right procedures and under the right circumstances cameras can be calibrated and then used some period of time later with

excellent results. In this particular case the results are broadly in line with the results that would be obtained if the cameras had been calibrated during the procedure.

5.10. Conclusions

Table 5.13 illustrates in general terms the methods that might be applied to obtain a certain level of accuracy.

Requirement	Recommendation	Section
Principal point location to +/- 1 pixel	Laboratory calibration using laser	4.3 & 5.1
Radial lens distortion correction to +/- 0.5 pixel	Use straight lines at the edge of the image format	4.5 & 5.2
Calibration of large format film cameras on the job	Goniometers, muli-collimator arrays, 3-D test fields, or use straight line features such as building facades, or railway lines	4.2-4.5 & 5.3-5.7
Calibration of analogue or digital cameras to +/- 0.1 pixel	Plumb line method coupled with laboratory location of the principal point	4.5 & 5.8
Calibration of analogue or digital cameras to the highest possible accuracy	Use 2-D or 3-D test fields for a full 3-D calibration procedure	4.4 & 5.9

Table 5.13. Recommended techniques to achieve specific objectives

In general terms there are only two practical methods for camera calibration, the first is the plumb line method that is simple and direct. The second is the full 3-D calibration method. The plumb line method is recommended when it is impossible to do a full 3-D calibration. The 3-D method is recommended for all cases even when the accuracy requirement is not of the highest level. By standardising on two essentially simple methods it should be possible to support camera calibration is most circumstances.

A final point is that neither of the two methods recommended is currently generally available cheaply or widely. The software for the 3-D method can be obtained under a different guise – i.e. for 3-D measurement purposes, the plumb line calibration routines are rarer and the authors do not know of a commercially available package that provides this function. It is thought that this lack of availability and the general lack of understanding of these techniques are reasons why they are not generally used. While the operation of the methods is both simple and relatively easy if the right procedures are followed, writing the software is only a job recommended for the proficient mathematician and software programmer. As a result of this difficulty users will often choose simpler and less adequate calibration methods. It is therefore recommended that the two methods discussed are documented and pseudo-code written suitable for implementation in any language or software package such as Mathcad. In addition a software package could be developed that would provide a set of camera calibration tools. By adopting two approaches both the expert and non-expert user could be catered for and the use of the techniques would not be dependent on a single software vendor.

5.11. References and Bibliography

Beyer, H.A., 1992, "Geometric and Radiometric Analysis of a CCD camera based Photogrammetric Close Range System", PhD thesis, Institut für Geodäsie und Photogrammmetrie, Zurich, Switzerland, May ,186 pages.

Carman, P. D. and H. Brown, 1956. Differences between visual and photographic calibration of air survey cameras. *Photogrammetric Engineering*. 22(4): 623.

Clarke, T. A. 1997. Spherical ball retro-reflective materials, Technical Report for Peter Cook PLC, 72 pages.

Clarke, T. A. Cooper, M. A. R. and Fryer, J. G., 1993. An estimator for the random error in subpixel target location and its use in the bundle adjustment. *Optical 3-D measurements techniques II*, Pub. Wichmann, Karlsruhe:161-168.

Hothmer, J. 1958. Possibilities and limitations for elimination of distortion in aerial photographs. *Photogrammetric Record*, Vol. II, No 12. pp. 426-445.

Karara, H.M., 1989, "Non-Topographic Photogrammetry", 2nd Ed., *Amer. Society for Photo. and Remote Sensing*, pp. 445.

Mikhail, E. M., 1981. *Analysis and Adjustment of Survey Measurements*. Van Nostrand Reinhold.

Fraser, C. S., 1996. Network Design. Chapter 9, *Close Range Photogrammetry and Machine Vision* (K.B.Atkinson, Ed.),Whittles, Scotland, 371 pages, pp. 256-282.

Shortis, M. R, Clarke, T. A., and Robson, S. 1995. Practical testing of the precision and accuracy of target centring algorithms. *Videometrics IV*, SPIE Vol. 2598, pp. 65-76.

Slama, C. C. (Ed), 1980. *Manual of Photogrammetry*. (Fourth Edition) American Society for Photogrammetry, Falls Church, Virginia, 1056 pages.

Topping, J. 1963. *Errors of observation and their treatment*. Chapman and Hall Ltd. London. 119 pages.